# Static Performance of Hot Bonded and Cold Bonded Inserts in Honeycomb Panels

G. BIANCHI\* AND G. S. AGLIETTI

School of Engineering Sciences, University of Southampton, Southampton SO17 1BJ, UK

## G. RICHARDSON

Surrey Satellite Technology Limited, Tycho House, Surrey Research Park, Guildford GU2 7YE, UK

ABSTRACT: An investigation on the structural performance of inserts within honeycomb sandwich panels is presented. The investigation considers metallic inserts in all aluminum sandwich panels and emphasis is placed on the structural performance difference between hot bonded and cold bonded inserts. The former are introduced during panel manufacture while the latter are potted into existing panels. The investigation focuses on the static performance of the two insert systems subject to loads in the normal direction to the facing plane. The experimental part of the work presented involved carrying out pullout tests on hot bonded and cold bonded reference samples by loading them at a centrally located insert. The experimental results were compared with results from an analytical model and results from a finite element model. Contrary to what was expected it was found from the experiments that the cold bonded inserts outperformed the hot bonded inserts in terms of load carrying capability. From the finite element study it was found that this was mainly due to the difference in stiffness of the different filler materials used in the two insert systems.

**KEY WORDS:** inserts, sandwich composite, honeycomb.

# INTRODUCTION

HONEYCOMB PANELS ARE extensively used in spacecraft structures due to their high specific strength and specific stiffness properties. Because of the weakness of the honeycomb core the transmission of loads between

Journal of SANDWICH STRUCTURES AND MATERIALS, Vol. 13—January 2011

<sup>\*</sup>Author to whom correspondence should be addressed. E-mail: g.bianchi@soton.ac.uk Figures 1, 2, 4–10 and 12–16 appear in color online: http://jsm.sagepub.com

honeycomb panels and other structures or components is generally achieved via the introduction of hard points, often in the form of bobbin shaped metallic inserts (Figure 1). Inserts can be split into two important categories depending on the method of integration into the honeycomb panel; hence a distinction is made between hot bonded inserts and cold bonded inserts (Figure 2). Hot bonded inserts are integrated with foaming adhesive during sandwich panel production; whereas cold bonded inserts are potted with curing resin into an existing panel. For both insert designs the foaming adhesive and curing resin act as a filler material that distributes the loads from the insert to the surrounding sandwich structure. As can be seen in Figure 2, apart from the method of integration, hot bonded and cold bonded inserts also differ in terms of their arrangement within the sandwich structure.

A honeycomb panel incorporating hot bonded inserts is produced by laying down the inserts at the same stage as the honeycomb core, which has cutouts at the locations where the inserts are to be placed. These are laid on top of the bottom facing sheet, which is covered in a layer of adhesive film. The sandwich is completed by laying down a second layer of adhesive film and the top facing sheet over the honeycomb core and inserts.

Hence, in the hot bonded arrangement, the insert is bonded to both the top and bottom face sheets and the insert height is equal to the core height. A hot bonded insert may thus be also regarded as a through-the-thickness type insert. For the cold bonded method of integration a hole has to be drilled in the sandwich panel to allow for an insertion of the bobbin insert.



Figure 1. Al Bobbin insert.

The hole can be drilled as deep as necessary so the insert height does not have to be necessarily equal to the height of the honeycomb core. Hence, a through-the-thickness arrangement can also be obtained by using the cold bonded method of integration but normally this is used to produce either fully potted or partially potted insert arrangements where the insert height is smaller than the core height. In the present paper cold bonded inserts are treated as having either fully potted or partially potted arrangements.

The use of cold bonded inserts is favored by the European Space Agency (ESA), which has extensively investigated their performance, also making its findings available in its Insert Design Handbook (IDH) [1], a comprehensive manual focused on the design, manufacture, and testing of these inserts. On the contrary hot bonded inserts have not been studied to the same extent. Although inserts have been widely used in the aerospace industry, little material has been published on this field [1–5,7–12]. A brief review of some of the most noteworthy studies is presented in what follows.

In Thomsen [2] and Thomsen and Rits [3] a mathematical model, which incorporates the transverse flexibility of the core is used to analyze the behavior of inserts subject to out-of-plane loads. The model is used to investigate the differences in structural performance between through-the-thickness inserts and fully potted inserts. In Bozhevolnaya et al. [4] and Bozhevolnaya and Lyckegaard [5] an analytical model initially developed to describe local effects across core junctions [6] is adapted to study plywood inserts in PVC core sandwich panels. The adapted model is used to show that stress concentrations due to material discontinuities can be significantly reduced by using patch core or structurally graded inserts to provide a more gradual transition from insert to core. The effect of insert/core boundary geometry was further investigated by Lyckegaard et al. [7] using a finite element parametric study. Here a curved shape of the boundary was found to be most effective at

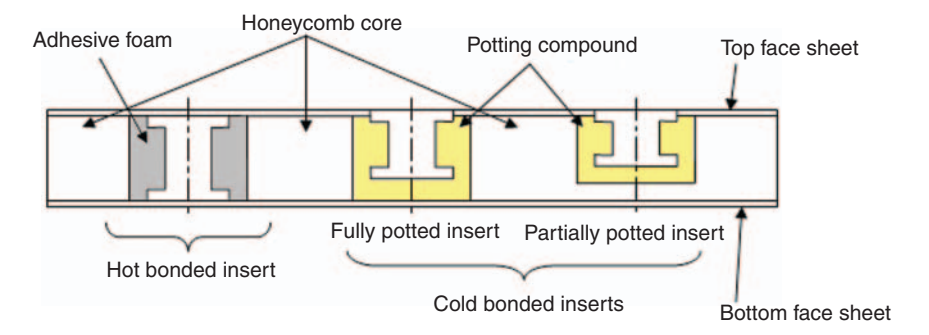


Figure 2. Illustration of inserts types used in honeycomb panels.

reducing stress concentrations. Bunyawanichakul et al. [8] carried out an experimental and numerical investigation on the performance of resin moulded inserts in aramid core sandwich panels relevant to aircraft structures and presented a numerical model, which includes the nonlinear behavior of the core. In Raghu et al. [9] the variability in pull-out strength of metallic inserts in aramid honeycomb sandwich panels is investigated and a higher variability is found for partially potted inserts. Kim and Lee [10] experimentally investigated the effect of insert shape on pull-out strength. Song et al. [11] carried out an experimental study to investigate the effect of various design variables (e.g., core height and density, skin thickness, etc.) on metallic inserts in aramid core sandwich panels with CFRP skins.

Apart from an early work from the present authors [12] most of the published works only deal with cold bonded inserts and hence here a more in depth study on both hot bonded and cold bonded inserts was conducted to assess their performance and effectively compare the two insert systems.

The experimental part of the investigation involved carrying out pull-out tests on honeycomb panel coupons by loading them at a centrally located insert. A large number of hot bonded and cold bonded reference samples were tested in order to identify failure mechanisms and produce data samples for comparison. These data were also compared with the results obtained from an analytical model proposed in the IDH. A finite element model was also developed in order to evaluate the stresses generated by pull-out loads throughout the insert system and surrounding sandwich structure.

#### INSERT CAPABILITIES

# Load Types and Strength Capabilities

The insert system can be subjected to the following five basic types of loads: (a) load normal to the plane of the sandwich away from the surface 'tensile load,'; (b) load normal to the plane towards the surface 'compressive load'; (c) load parallel to the sandwich facing 'shear load'; (d) bending load; and (e) torsional load. These may act alone or in combination, but design should favor the first three load types since inserts are not suited to carrying bending and torsional loads. Torsional loads in particular should be just limited to screwing and locking torques only. This represents a potential area of improvement in insert design; however, excessive bending and torsional loads can be easily avoided by using insert groups to convert moments into simple forces, which are either parallel or normal to the insert axis

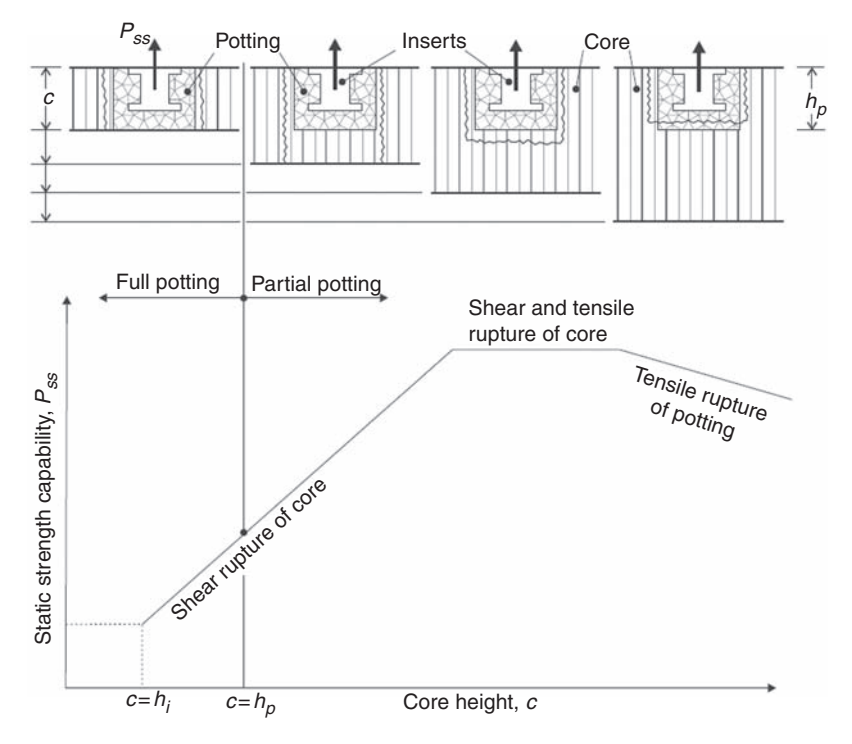


Figure 3. Influence of core height on failure modes.

(e.g., bending loads can be avoided by using coupled inserts which convert the load to normal tension/compression).

The normal tensile and compressive load-carrying capabilities are the most important strength parameters in defining the structural performance of inserts. In the IDH strength data regarding the structural performance of cold bonded inserts is limited to normal tensile and compressive loads, and the literature available on the topic of inserts in general is only concerned with these two load types. The work here presented is focused on the static strength capability of inserts subject to normal tensile loads.

# Failure Modes Under Normal Tensile Loads

In the IDH [1] it is shown that, for a given potting height  $h_p$ , the decisive failure modes affecting the static strength capability  $P_{SS}$  of a cold bonded insert subject to a normal tensile load are primarily influenced by the core height c. In the graph shown in Figure 3 it can be seen how the  $P_{SS}$  of a cold bonded insert varies with core height. Looking at the  $P_{SS}$  curve it is possible

to split the graph into three areas, each of which associated with a failure mode. In the first part of the graph, starting from  $h_i = c$ , the  $P_{SS}$  increases quasi-linearly with core height. Here the insert system fails by shear rupture of the core surrounding the insert so the property limiting the  $P_{SS}$  is the shear strength of the core. The  $P_{SS}$  increases quasi-linearly with core height because of the corresponding increase in area over which the shear load is distributed. As the core height increases the insert becomes partially potted and the core underneath the potting is subjected to tensile stress. When  $c-h_n$ reaches a critical value the tensile stress underneath the potting reaches the tensile strength of the core, and the second failure mode (coinciding with the second part of the graph) comes into effect. Now the insert fails by the combination of shear rupture of the core around the potting and tensile rupture of the core underneath the potting occurring together: the  $P_{SS}$  is then simultaneously limited by the core shear strength and the core tensile strength and, as illustrated in the second part of the graph, is almost independent of further increases in core height. This is because due to the rigidity of the potting only part of the full core shear strength is used (i.e., the critical shear strength of the core is not reached). The load part carried by shear stresses in the core around the potting decreases with the core shear stress as c increases.

The potting underneath the insert is also subjected to tensile stress which increases with core height. If this stress exceeds the tensile strength of the potting compound before the tensile strength of the core is reached the insert will fail by tensile rupture of the potting. This is likely to occur for strong cores when a certain core height is reached. As can be seen in the graph, for this third failure mode, further increases in core height result in a mild decrease in  $P_{\rm SS}$ .

The outer diameter of the insert (i.e., the diameter of the flanges) has a major influence on the  $P_{SS}$  for all the failure modes discussed above. This is because it determines the potting radius and consequently the area over which shear loads are distributed over the walls of the surrounding core, and because it determines the area underneath the insert and the potting over which normal tensile loads are carried.

If this failure mode criteria proposed in the IDH is applied to hot bonded inserts as well it can be said that, because the insert height  $h_i$  is always equal to the core height  $h_c$ , shear rupture of the core around the insert should be the only relevant failure mode for this inserts type and that static strength capability should always increase quasi-linearly with core height. It follows that, for equivalent insert outer diameter, equivalent core specification and equivalent core height, the static strength capability of a hot bonded insert should be very similar to that of a fully potted cold bonded insert. However, because the insert is bonded to both the face sheets,

the through-the-thickness design of a hot bonded insert looks and is generally recognized as being stronger than the fully potted design. To actually determine the performance difference between the two designs, the experimental study involved carrying out pull-out tests on hot bonded coupons and fully potted cold bonded coupons.

#### MATERIAL SPECIMENS

Hot bonded insert coupons and fully potted cold bonded insert coupons were produced in order to conduct pull-out tests. To ensure a relevant comparison the same sandwich panel specifications were used for both of these coupon types. The sandwich structure consisted of two 2014 aluminum alloy face skins 0.5 mm in thickness, sandwiching a 19 mm thick aluminum core, designated as  $\frac{1}{4}$ " – 5056 – 0.0025" (which should be read as: cell size in inches – Al alloy – foil thickness in inches), 6.35 mm in cell size and 83 kg/m³ in density. All reference samples had dimensions  $80 \times 80 \times 20 \text{ mm}^3$ . The face skins were bonded to the honeycomb core using Redux 319 adhesive film.

The hot bonded insert coupons (Figure 4(a)) incorporated a centrally located aluminum bobbin insert, 16 mm in outer diameter, 19 mm in height (i.e., same height as the core). The inserts were originally introduced in the sandwich structure during panel manufacture using Redux 219/2-NA foaming film adhesive as the filler material. This is an epoxy based foaming adhesive, initially presented as sheet film, which after application expands upon curing by a ratio in the range from 1:19 to 1:1.4. In this installation

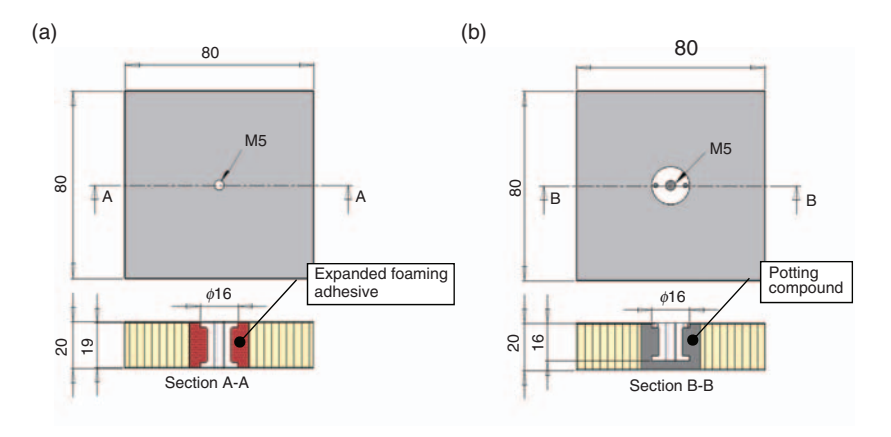
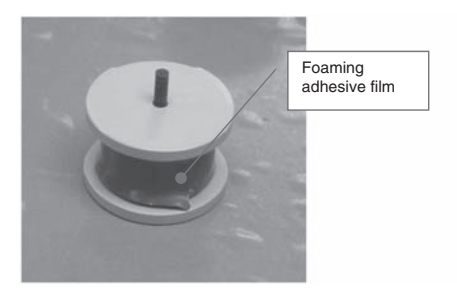


Figure 4. Dimensioned drawings of coupons: (a) hot bonded coupon and (b) cold bonded coupon.





**Figure 5.** Installation procedures for (a) example of a hot bonded insert laid down with a film of foaming adhesive during sandwich panel manufacture and (b) injection of potting compound during cold bonded insert installation.

procedure a few layers of foaming film adhesive are wrapped around the bobbin insert (Figure 5(a)) before laying it down. The foaming adhesive then expands during curing of the sandwich panel to fill the cavity between the bobbin and the surrounding walls of the open core cells.

For the cold bonded coupons (Figure 4(b)) aluminum bobbin inserts were potted at the center of sandwich panel squares cut to match the dimensions specified above. Here, the inserts were potted in the coupons using Stycast 1090 as the potting compound. This is an epoxy-based encapsulant, which is liquid when applied and then hardens upon curing without expanding (the product is actually quoted as having low cure shrinkage). In this installation procedure the bobbin is inserted in the machined hole and then, as its top flange is maintained flush with the top surface of the panel, the potting compound is squirted via one of the holes in the flange to fill the cavity (Figure 5(b)). A second hole is required to allow for venting. The outer diameter has a major influence on  $P_{SS}$  so in order to ensure a relevant comparison with the hot bonded reference samples the bobbin inserts used here were also 16 mm in outer diameter. Again to maintain a relevant comparison a fully potted arrangement was chosen since, according to the existing insert capabilities theories described earlier, the failure mode should be the same as for the hot bonded configuration. To obtain a fully potted arrangement bobbin inserts 16 mm in height were used for the cold bonded coupons.

For both coupon types the bobbin inserts were made in 6082 aluminum alloy and the mechanical connection could be achieved through an M5 threaded hole at the center of the bobbin.

## EXPERIMENTAL PROCEDURE

All the coupons were subjected to pull-out tests using an Instron 8802 universal servo-hydraulic testing machine. The machine is equipped with a



Figure 6. Al-alloy test fixture with 70 mm diameter circular cutout.

100 kN load cell and an LVDT incorporated in the lower crosshead. The load and crosshead signals were recorded through an external PC using the DasyLab data acquisition system. The testing was conducted at room temperature and in accordance with ESA guidelines outlined in the IDH. To comply with these guidelines a specifically designed test fixture (Figure 6) was used to hold the samples and expose a free circular area 70 mm in diameter around the insert. The set-up used for all the tests was installed in the Instron machine as shown in Figure 7 and is described as follows: An M5 bolt is connected to the reference sample via the female threaded part of the insert. The shank of the bolt is contained within a rectangular steel block, which can be clamped into the hydraulic grips of the upper crosshead. The lower part of the test fixture has a hole in which a headed steel dowel pin is inserted. The cylindrical body of the pin can be clamped into the hydraulic v-grips of the lower crosshead. Once the described set-up was achieved, starting from an unloaded condition, the specimens were loaded at constant crosshead displacement rate of 1 mm/min until ultimate failure occurred. During the tests load data and crosshead displacement data were recorded at a sampling rate of 10 Hz.

## **EXPERIMENTAL RESULTS**

A total of 23 hot bonded and eight cold bonded coupons were tested as described above. Typical load versus crosshead displacement curves

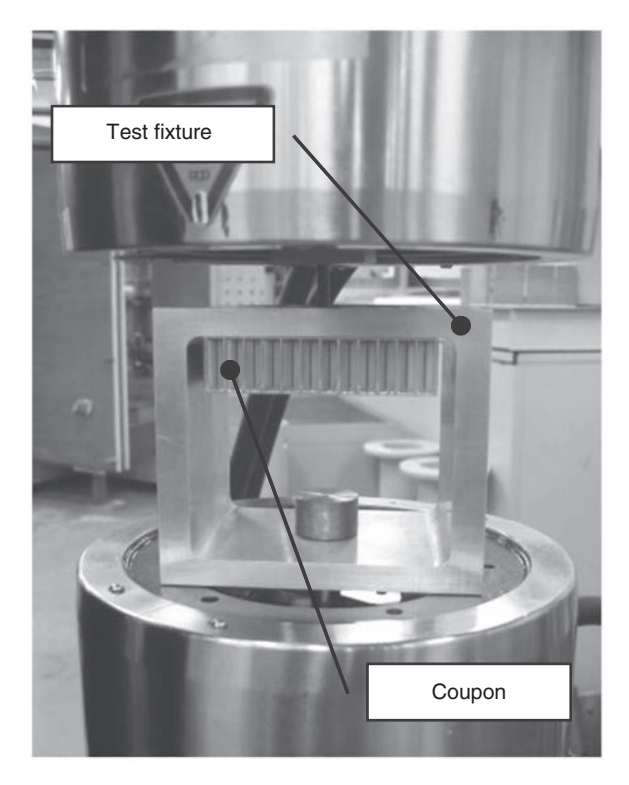


Figure 7. Arrangement of the coupon and test fixture installed between the crossheads of the universal testing machine.

obtained for both tested insert types are shown in Figure 8. Based on the behavior of these load—displacement curves it is possible to split the plot into three regions. In the first part of the plot the curves are nonlinear, which is probably a result of the establishment of contact between the coupons and the test fixture. In the second part of the plot the curves show a nearly linear behavior indicating that near elastic deformation is taking place and that no significant damage is occurring. In the third part of the plot the curves are nonlinear due to the progressive damaging of the insert systems. Here, as damage takes place the slope of the curves progressively reduces until peak load is reached. Finally, the damage is so great that most of the strength is lost and the load—displacement curve drops sharply. From the linear part of the curves it can be seen that the slope is steeper for the cold bonded coupon. This was the case for all the tested coupons and is an indication that the overall insert system stiffness was higher for the cold bonded coupons.

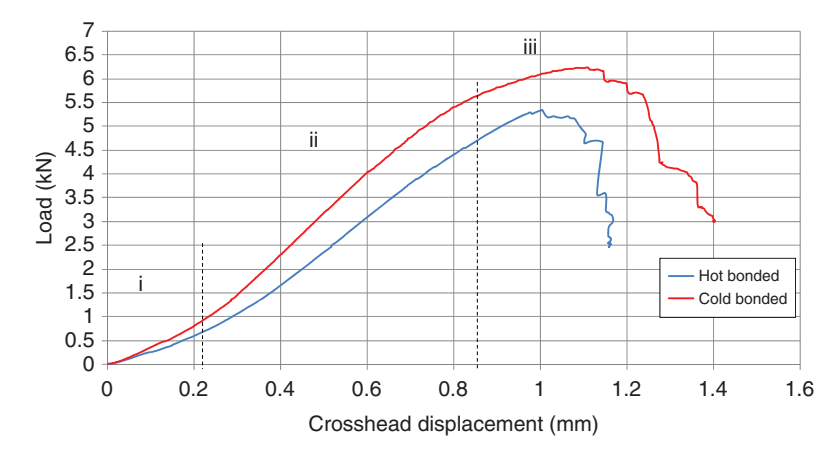


Figure 8. Typical load Vs crosshead displacement curves for hot bonded and cold bonded coupons.

From the plot it can be seen that the cold bonded insert coupons failed at a higher load than the hot bonded insert coupons. For all the tested coupons the insert static strength capability was taken as the peak load from the obtained load–displacement curves. The average static strength capability,  $P_{SS,av}$ , obtained for the hot bonded coupons was 5.6 kN and lower than the  $P_{SS,av}$  of 6.18 kN obtained for the cold bonded coupons. These results are shown in Table 1, which also includes the standard deviations.

After testing some of the reference samples were sectioned across the center in order to check the manufacturing quality and identify failure modes (Figure 9 and 10).

By visual observation, it is evident that, for both the hot bonded and the cold bonded coupons, failure initiates in the core by shear buckling of the cell walls. However, this does not cause an immediate load drop since, initially, the diagonal cell buckling will produce a diagonal (Wagner) tension field which still retains load carrying capacity. This is confirmed later on by comparing these experimental results with those obtained in the numerical study and the shear buckling instability calculation presented in the section 'Numerical Study.' This post-buckling phase is likely to correspond to the relatively gradual drop in stiffness that can be observed in Figure 8 between regions ii and iii. Eventually, as the yield strength is reached the cell walls lose their structural integrity leading to the sudden load drop that can be seen in region iii.

No manufacturing defects were detected in the sectioned coupons.

	Hot bonded	Cold bonded	
$P_{SS,av}$ (kN)	5.60	6.18	
No. of samples	23	8	
Standard deviation	0.46	0.29	

Table 1. Experimental results.



Figure 9. Image of a hot bonded reference sample sectioned after testing.



Figure 10. Image of a cold bonded reference sample sectioned after testing.

# THEORETICAL STUDY OF TESTED INSERT SYSTEMS

The IDH contains a vast range of data concerning the normal tensile and compressive strength capabilities of cold bonded inserts. These data are presented in the form of diagrams, which for a given core type and insert size; show how the minimum and average load carrying capability values vary with core height.

The honeycomb cores for which diagrams have been produced were 0.02 or 0.03 mm in foil thickness and 3.2 or 4.8 mm in cell size; however, the honeycomb core used for the experimental work described here is heavier

with 0.06 mm foil thickness and 6.35 mm cell size so these diagrams are not directly applicable.

The diagrams are not generated from direct experimental data but are actually produced using an analytical method, which has been compared with test results to verify its validity and produce reliability coefficients. Hence, using this method it is possible to generate a diagram relevant to the core type used in the tested reference samples. The analytical approach is based on an analytical model proposed in Ericksen [13] which provides a means of determining the radial distribution of shear stress  $\tau(r)$  in a sandwich panel that is loaded normal to the facing plane, and an empirical formulation from MIL-HDBK 23 A [14] which can be used to determine the radial position of maximum shear stress,  $r_{\tau, \text{max}}$ . From these works, using  $\tau(r)$  and  $r_{\tau, \text{max}}$ , in the analytical approach proposed by the IDH the maximum shear stress in the core is given by:

$$\tau_{\text{max}} = \frac{P}{2\pi bc} \frac{\beta}{\beta + 1} K_{\text{max}},\tag{1}$$

where P is the applied load, b is the potting radius, c is the core height and  $\beta$  is the core height to face skin thickness ratio c/f. K is a parameter which depends on the radial position from the center of load application. K is equal to  $K_{\max}$  at the position of maximum core shear stress  $r_{\tau,\max}$  (an expression for this is also shown in the Appendix).

If the failure mode is by shear rupture of the core then failure will occur when the load is such that  $\tau_{\text{max}}$  exceeds the circular shear strength of the core  $\tau_{C,crit}$ . The above expression can be directly used to determine the insert capability by rearranging as follows:

$$P_{crit} = \frac{2\pi b c \tau_{C,crit}}{C * K_{max}},\tag{2}$$

with  $C^* = \beta/(\beta + 1)$ .

This expression will normally apply to through-the-thickness, fully potted inserts and partially potted inserts with a small  $c-h_p$  value. However, as seen in the section 'Failure Modes under Normal Tensile Loads,' for partially potted inserts with a large  $c-h_p$  value failure is more likely to occur due to rupture of the core underneath the potting or rupture of the potting underneath the insert (for heavier cores). In these cases the insert capability cannot be described by Equation (2) alone since other load contributions need to be considered. For a partially potted insert in aluminum core the load applied to the insert consists of three parts: (i) load applied to the upper facing; (ii) load part carried by shear stresses in the core around the potting, (iii) load part carried by normal stresses in the core underneath the potting.

Theoretically shear rupture of the core and tensile rupture of the core should not occur together. However, the IDH states that due to nonlinearity effects  $\tau_{C,crit}$  and  $\sigma_{C,crit}$  are actually reached simultaneously. Hence by combining the load contributions it is possible to show [1] that the capability of a partially potted insert is given by:

$$P_{p,crit} = \frac{1}{2} P_{crit} + \pi r_{\tau,\max} (2h_p - c) \tau_{C,crit} + \pi r_{\max}^2 \sigma_{C,crit},$$
 (3)

where  $\sigma_{C,crit}$  is the tensile or compressive circular strength of the core (depending on whether the load is tensile or compressive).

For a partially potted insert in a heavy aluminum core failure is more likely to occur in the potting and hence the relevant load contributions are different. These can still be divided in three parts: (i) Load applied to the upper facing; (ii) load part carried by shear stresses in the core around the potting over the insert height; (iii) load part carried by normal stresses in the resin underneath the insert. By combining these load contributions it is possible to show [1] that the capability of a partially potted insert in heavy aluminum core is given by:

$$P_{R,crit} = \frac{2P_{NR,crit}}{1 + \frac{(c - 2h_t)r_{t,max}}{ch}C * K_{max}},$$
(4)

where  $P_{NR,crit}$  is the critical load that can be carried by normal stresses in the resin underneath the insert and is given by:

$$P_{NR,crit} = \pi b_R^2 \sigma_{R,crit},\tag{5}$$

where  $b_R$  corresponds to the real potting radius and  $\sigma_{R,crit}$  is the critical tensile strength of the resin.

Equations (2)–(4) can be used to predict the capability and the failure mode of a given insert system. These equations should be used as follows: if the insert is through-the-thickness or fully potted then its capability will be described by  $P_{crit}$  for a partially potted insert the decisive failure mode is not certain so  $P_{crit}$ ,  $P_{p,crit}$ , and  $P_{R,crit}$  should all be evaluated. The lowest out of the three values obtained will represent the actual insert capability  $P_{SS}$  and indicate the mode of failure. Minimum or average values of  $P_{SS}$  can be calculated using Equations (2)–(4) by prescribing minimum or average values of potting dimensions  $(b, b_R, h_p)$ , core properties  $(\tau_{C,crit}, \sigma_{C,crit})$ , and potting material strength  $(\sigma_{R,crit})$ . The final  $P_{SS}$  value is determined by multiplying by reliability coefficients found in the IDH, which have been determined by comparing the model with test results. The resulting minimum  $P_{SS}$  values are regarded as A-basis values meaning that 99% of specimens are expected to exceed this value with a confidence level of 95%.

Table 2. Minimum and typical critical values used for the honeycomb core and the potting material.

	Honeycomb core <sup>a</sup>		Filler/Potting material <sup>b</sup>	
	Circular shear strength (Mpa)	Normal tensile strength (Mpa)	Tensile strength (Mpa)	
Min Typical	2.30 2.81	9.34 10.38	14 18	

<sup>&</sup>lt;sup>a</sup>Honeycomb core property values sourced and derived from ESA Composite Design Handbook [15]. <sup>b</sup>Potting material values sourced from manufacturer quoted values for Stycast 1090.

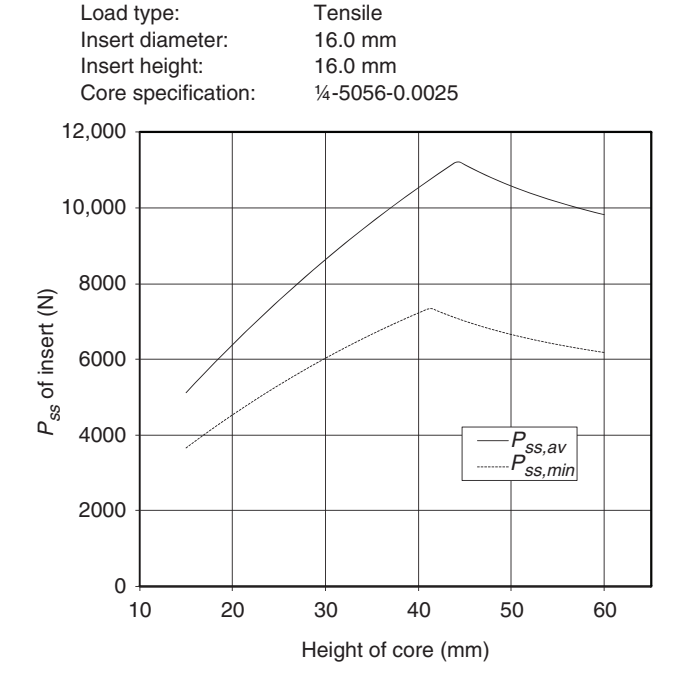


Figure 11. Load-carrying capability plot produced using the analytical model with the parameters of tested cold bonded samples.

Implementing this analytical approach it was possible to accurately reproduce the diagrams shown in the IDH. By using the appropriate parameters and material properties (Table 2) it was thus possible to generate a diagram for the core specifications and insert dimensions used for the tested cold bonded insert reference samples (Figure 11). From the diagram it is possible

to see that for a core height of 19 mm the behavior of both curves is still quasi-linear indicating that the model predicts shear rupture of the core around the potting as the failure mode. The predicted average  $P_{SS,av}$  value is  $6.14 \, \mathrm{kN}$  and the minimum  $P_{SS,\mathrm{min}}$  value is  $4.38 \, \mathrm{kN}$ .

The diagram in Figure 11 was produced for an insert height of 16 mm. However, the IDH states that the diagram would also be applicable to other  $h_i$  values. The insert height only controls the break of the curves, where the quasi-linear behavior stops and the failure mode changes. For higher  $h_i$  values the curve break occurs at higher core height values and vice-versa. At a core height of 19 mm (i.e., the hot bonded insert configuration) the behavior of the curves would still be quasi-linear and indicate the same load carrying capability values  $P_{SS,av} = 6.14$  kN and  $P_{SS,min} = 4.38$  kN. This means that the analytical model does not distinguish between the hot bonded and cold bonded reference samples. The reason for this is that in the formulation proposed by Ericksen only the shear stress distribution through the sandwich core is considered and the normal load is assumed to be applied over a rigid circular disk which the IDH adaptation has a radius equal to the potting (filler material) radius. Hence, for the core shear stress mode of failure the IDH model does not consider the insert system geometry or the stiffness of the filler material.

Both these analytical results and the average static strength capability results obtained from the experiments are summarized in Table 3. For average static strength capability values there is a very good correlation between the analytical result and the experimental result obtained for the cold bonded coupons, while for the hot bonded coupons the experimental average is about 10% lower. The reason for the latter discrepancy was found by conducting a numerical study and is explained in the section 'Finite Element Model Results.'

# **NUMERICAL STUDY**

# **Description of the Finite Element Models**

An investigation using the finite element method was conducted in order to determine why the fully potted cold bonded insert coupons outperformed

Table 3. Summary of experimental and analytical results.

the hot bonded insert coupons. Because failure initiates in the core, the structural performance of the two insert systems can be compared by looking at the behavior of the honeycomb cell walls. However, rather than going through the complexities of attempting to predict the exact buckling loads via a computationally expensive nonlinear analysis, here the approach that was taken was to use a simpler and more reliable linear analysis to look at the magnitude of the stress fields generated in the honeycomb cell walls. Two models corresponding to the two coupon types were created in Patran and solved using Nastran (Figure 12(a) and (b)). Using symmetry constraints it was possible to model only one half of the coupons. The detailed 3D geometry of the honeycomb core was modeled using quadrilateral shell elements. The modeling of this part was based on the  $\frac{1}{4}$ "-5056-0.0025" core used for both coupons and included the double wall thickness along the ribbon direction. The face skins were also modeled using quadrilateral shell elements. The insert, adhesive foam and potting compound were all modeled using quadrilateral brick elements.

Figure 13 shows the constraints that were applied to the model in order to simulate the pull-out test conditions. The nodes corresponding to a circular strip 35 mm in inner radius and one element wide were constrained in the out-of-plane direction to simulate the constraint provided by the test fixture. The out-of-plane load applied via the fastener was modeled using a multi-point constraint (MPC). In order to compare the two models with the experimental results a load of 5 kN close to the average static strength capability achieved for both insert coupons was applied in the simulations.

The material properties entered in the models for the aluminum parts of the coupons are shown in Table 4. For the potting compound (Stycast 1090) the manufacturer quotes the elastic modulus as being in the range 2400–2500 MPa.

An elastic modulus for the adhesive foam (Redux 219/2-NA) could not be obtained from the manufacturer so a compressive test on a cylindrical

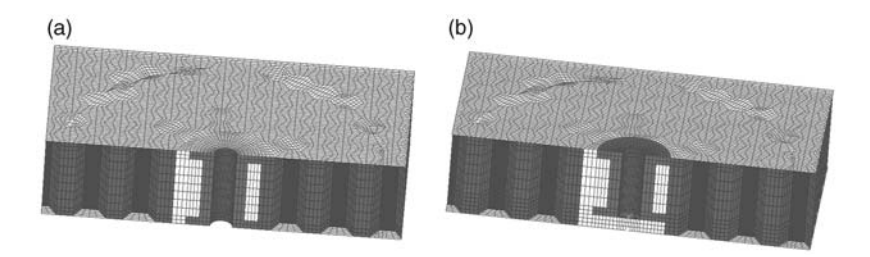


Figure 12. Meshing of the finite element models: (a) hot bonded coupon model and (b) cold bonded coupon model.

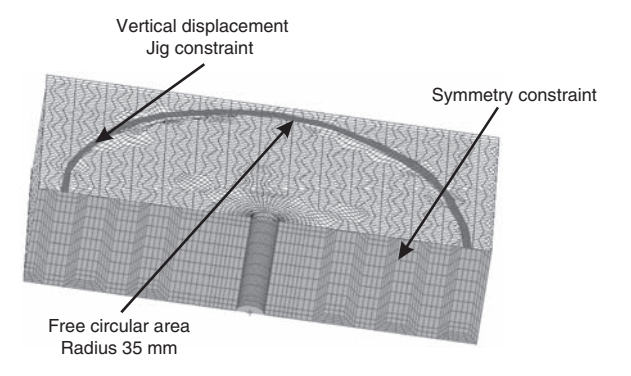


Figure 13. Boundary conditions.

Table 4. Material properties used in the finite element models for Al-alloy parts.

	Material	Young's modulus, <i>E</i> (MPa)	Poisson's ratio, υ	Shear modulus, G (MPa)
Face skins	Al 2014	72,400	0.33	27,218
Honeycomb cell walls	Al 5056	70,300	0.33	27,038
Bobbin insert	Al 6082	68,300	0.33	25,676

sample was conducted to measure this property (Figure 14). The test was conducted in displacement control using screw driven Instron 5559 testing machine. The deformation of the sample was accurately measured using an extensometer and an elastic modulus of 1034 MPa was obtained from the test. However, due to the variability of the expansion ratio of the adhesive foam (1:1.19–1:1.4), this should only be taken as an indication of the elastic modulus that that may be expected. Empirical data found in Gibson and Ashby [16] suggests that for a foam with a relatively low expansion ratio (<1:1.6) the following relationship applies:

$$\frac{E^*}{E_s} \approx \left(\frac{\rho^*}{\rho_s}\right)^2,\tag{6}$$

where  $E^*$  and  $E_s$  are the elastic moduli of the foam material in its expanded and solid (unexpanded) state respectively; and  $\rho^*/\rho_s$  is the relative density of the foam cell which corresponds to the expansion ratio. The expansion ratio of the adhesive foam cannot be controlled and hence the elastic modulus is



Figure 14. Compressive test of Redux 219/2-NA adhesive foam.

likely to vary considerably from case to case depending on how open cells of the honeycomb core are filled. According to Equation (6) the ratio  $E^*/E_s$  can vary from 0.51 to 0.70 for the quoted expansion ratios.

The elastic modulus of the filler material (potting compound or adhesive foam) plays an important role in determining how the external insert loads are transmitted to the surrounding sandwich structure. For this reason, and to address the variability in expansion ratio of the adhesive foam, a filler material elastic modulus sensitivity study was conducted for both model geometries. The Stycast 1090 maximum elastic modulus of 2500 MPa was taken as the upper bound of the study and simulations were run in decreasing steps of 500 MPa down to 500 MPa. In both cases the potting compound and the adhesive foam were assumed isotropic with a Poisson's ratio of 0.3 and the shear modulus was obtained using the expression G = E/2(1 + v).

### **Finite Element Model Results**

Since for both coupon types the decisive failure mode was in the honeycomb core the main focus of the sensitivity study was on how the elastic modulus of the filler material affected the stresses generated in the cell walls. Figure 15 shows a contour plot of the maximum principal stresses generated in the cell walls of the core obtained for the hot bonded model with an elastic modulus of 2500 MPa entered for the adhesive foam. Apart from the magnitude of the stresses the distribution of the stresses did not vary significantly between the two models or the filler material stiffness. As can

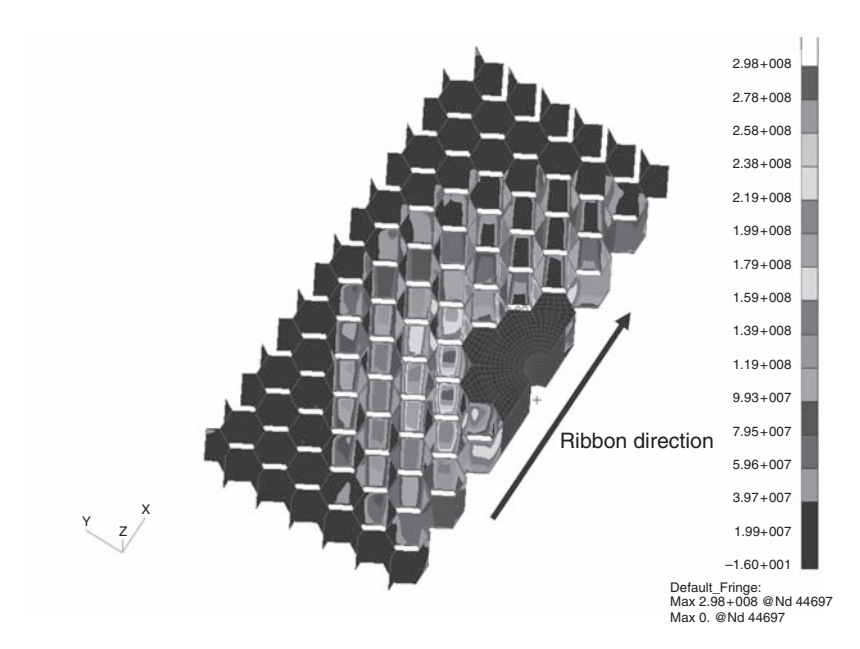


**Figure 15.** Contour plot of maximum principal stresses generated in the cell walls of the core (face skins are hidden).

be seen in Figure 15 the single thickness cell walls closest to the filler material (adhesive foam in this case) are subjected to the highest stress levels. Figure 16(a) and (b) illustrate how the generated maximum principal stresses and shear stresses in the cell walls varied between the hot bonded and cold bonded model and how they were affected by the filler material stiffness.

From Figure 16(a) and (b) it can be seen that the variations in maximum principal and shear stress between the hot bonded model and the cold bonded model are small compared to the variations due to changes in filler material stiffness. For values of filler material stiffness above 1000 MPa the results show that for the hot bonded insert geometry the stresses are slightly lower than for the cold bonded insert geometry. However, the results show that the impact of the filler material stiffness is significantly greater with a substantial decrease in stress levels with decreasing stiffness. For both models an increase of almost 10% in maximum principal and maximum shear stresses is obtained when the filler material stiffness decreases from 2500 to 1000 MPa. Assuming a relationship between the magnitude of these stresses and insert failure load then the increase in these stress levels is comparable to the difference in static load carrying capability obtained between the tested hot bonded and cold bonded

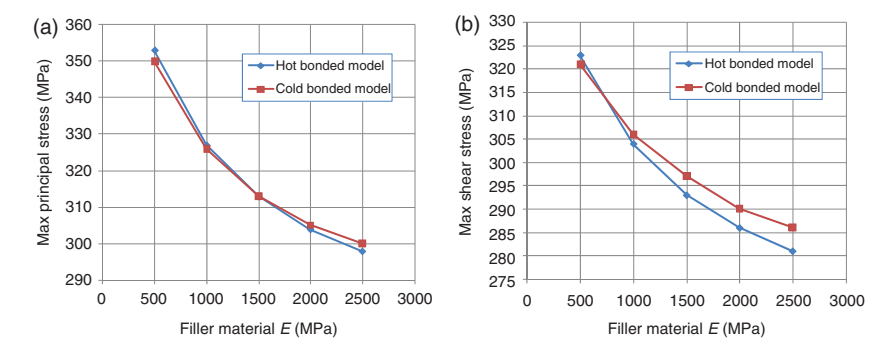


**Figure 16.** Plots showing variation of stresses in cell walls with filler material stiffness for an insert pull-out load of 5 kN: (a) variation of max principal stress with filler material stiffness and (b) variation of max shear stress with filler material stiffness.

coupons. The measured elastic modulus for the Redux 219/2-NA adhesive foam was close to 1000 MPa so the difference in filler material stiffness (even accounting for expansion ratio variation) is probably the main cause of the lower average load carrying capability that was obtained in the experimental results for the hot bonded coupons.

# **Shear Buckling Instability Calculation**

In order to further investigate the failure process in the honeycomb core a formula for the shear buckling strength of thin plates proposed by Roark and Young [17] was applied to the single thickness inclined wall of the core and the results compared with the maximum shear stresses plotted in Figure 16. The buckling strength of a single thickness cell wall can be expressed as:

$$\tau^{cr} = K_{cr} \frac{E}{1 - v} \left(\frac{t}{l}\right)^2,\tag{7}$$

where  $K_{cr}$  is a factor that depends on the length to width ratio of the plate and how its constrained, t is the thickness of the cell wall, l is the length of the cell wall, and E and v are the elastic modulus and the Poisson's ratio. For the dimensions of the cell wall  $K_{cr} = 4.4$  for a simply supported constraint and  $K_{cr} = 7.38$  for a fully clamped constraint. In actual fact the cell wall is neither simply supported nor fully clamped but somewhere in between the two conditions, and hence it is appropriate to calculate the critical shear stress  $\tau^{cr}$  for both cases. It can be found that for the simply supported case  $\tau^{cr} = 67.9 \, \text{MPa}$  while for the fully clamped case

 $\tau^{cr}$  = 113.8 MPa. Both of these values are significantly lower than the maximum shear stress values plotted in Figure 16(b). Considering that the finite element shear stress values were calculated for a pull-out insert load close but below the maximum achieved in the experiments, it follows that the single thickness cell walls operate in a post-buckling regime when the insert system is subjected to high loads.

#### CONCLUSIONS

A study on hot bonded inserts has been conducted to assess their performance and compare them with cold bonded inserts. Contrary to what was expected the experimental results showed that the cold bonded fully potted inserts outperformed the hot bonded inserts in terms of static strength capability. However, as expected, in both cases failure initiates in the honeycomb core by shear buckling of the cell walls. The results from the finite element study showed that the unexpectedly lower performance of the hot bonded inserts can be attributed to the stiffness of the filler material. The adhesive foam used as the filler material for the hot bonded inserts has a sensibly lower stiffness than the potting compound used in the cold bonded inserts and hence is less effective at transmitting external insert loads to the surrounding honeycomb core in an even manner. For equal filler material stiffness the finite element results showed that the hot bonded insert design performs slightly better than the cold bonded fully potted design.

The comparison of results from buckling theory on thin plates subject to uniform shear loads with the results obtained from the finite element model shows that when the insert is subject to high loads the inclined single thickness cell walls operate in a post-buckling regime from which recovery is still possible once the load is removed.

An analytical model proposed in the IDH was also applied to the tested insert systems and a good correlation was found with the experimental cold bonded insert results. However, due to its simplifying assumptions the model cannot distinguish between the hot bonded and the fully potted cold bonded design.

# **NOMENCLATURE**

 $C^* = \beta/(\beta+1)$ 

E =Young's modulus

K =symbol used for compact notation in core shear stress distribution formula

 $K_{\text{max}}$  = value of K at position of maximum core shear stress  $r_{\tau,\text{max}}$ 

 $K_{cr}$  = shear buckling instability factor

P = load applied at insert normal to facing plane

 $P_{SS}$  = static strength capability of insert

 $P_{crit}$  = insert capability for shear core failure

 $P_{p,crit}$  = insert capability for failure of the core underneath the potting

 $P_{R,crit}$  = insert capability for failure of the potting underneath the insert

 $P_{NR}$  = load carried by tensile stresses in potting compound

 $P_{NR,crit}$  = critical load carried by tensile stresses in potting compound

b = potting radius

 $b_R$  = real potting radius

c =core thickness

f =facing skin thickness

h = total sandwich thickness

 $h_i = \text{insert height}$ 

 $h_p$  = potting height

l = cell wall length

r = radial distance from insert center (point of normal load application)

 $r_{\tau,\text{max}}$  = radial position of maximum core shear stress

t = cell wall thickness

 $\beta = c/f$ 

v = Poisson's ratio

 $\tau_{C,crit}$  = circular shear strength of the core

 $\tau_{\rm max} = {\rm maximum} {\rm core} {\rm shear} {\rm stress}$ 

 $\sigma_{C,crit}$  = tensile or compressive strength of the core

 $\sigma_{R,crit}$  = tensile strength of the potting

#### REFERENCES

- ESA (1987). Insert Design Handbook, European Space Agency, ESA PSS-03-1202, Issue 1, Paris.
- Thomsen, O.T. (1998). Sandwich Plates with 'Through-the-Thickness' and 'Fully Potted' Inserts: Evaluation of Differences in Structural Performance, Composite Structures, 40(2): 159–174.
- 3. Thomsen, O.T. and Rits, W. (1998). Analysis and Design of Sandwich Plates with Inserts A High–order Sandwich Plate Theory, *Composites Part B*, **29**(6): 795–807.
- Bozhevolnaya, E., Lyckegaard, A., Thomsen, O.T. and Skvortsov, V. (2004). Local Effects in the Vicinity of Inserts in Sandwich Panels, Composites Part B, 35(6–8): 619–627.
- Bozhevolnaya, E. and Lyckegaard, A. (2004). Structurally Graded Core Inserts in Sandwich Panels, Composite Structures, 68(1): 23–29.
- Skvortsov, V. and Thomsen, O.T. (2002). Analytical Estimates for the Stresses in Face Sheets of Sandwich Panels at the Junctions Between Different Core Materials, In: Proceedings of the 6th International Conference of Sandwich Structures (ICSS-6), Fort Lauderdale, Florida, pp. 551–559.

 Lyckegaard, A., Bozhevolnaya, E. and Thomsen, O.T. (2006). Parametric Study of Structurally Graded Core Junctions, *Journal of Sandwich Structures and Materials*, 8(5): 423–435.

- Bunyawanichakul, P., Castanie, B. and Barrau, J.J. (2005). Experimental and Numerical Analysis of Inserts in Sandwich Structures, Applied Composite Materials, 12(3,4): 177–191.
- 9. Raghu, N., Battley, M. and Southward, T. (2008). Strength Variability of Inserts in Sandwich Panels, In: 8th International Conference on Sandwich Structures (ICSS 8), Porto.
- 10. Kim, B.J. and Lee, D.G. (2008). Characteristics of Joining Inserts for Composite Sandwich Panels, *Composite Structures*, **86**(1–3): 55–60.
- 11. Song, K.-I., Choi, J.-Y., Kweon, J.-H., Choi, J.-H. and Kim, K.-S. (2008). An Experimental Study of the Insert Joint Strength of Composite Sandwich Structures, *Composite Structures*, **86**(1–3): 107–113.
- 12. Bianchi, G., Aglietti, G.S. and Richardson, G. (2008). Static Performance of Hot Bonded Inserts in Honeycomb Panels, In: 49th AIAA/ASME/ASCE/AHS/ASC Structures, Structural Dynamics, and Materials Conference, Schaumburg, II, USA, 7–10 April.
- 13. Ericksen, W.S. (1953). The Bending of a Circular Sandwich Plate Under Normal Load, Forest Product Laboratory, Report No. 1828, Madison 5, Wisconsin.
- 14. MIL-HDBK-23 A (1968). *Structural Sandwich Composites*, Department of Defense, Washington, DC.
- ESA (1986). Composite Design Handbook, European Space Agency, ESA PSS-0301101, Paris.
- Gibson, L.J. and Ashby, M.F. (1988). Cellular Solids: Structure and Properties, Cambridge University Press, New York.
- Roark, R.J. and Young, W.C. (1975). Formulas for Stress and Strain, Pergamon Press, Oxford.